State Estimation for MRI-Actuated Catheters via Catadioptric Stereo Camera

Tipakorn Greigarn, Russell Jackson, M. Cenk Çavuşoğlu

Abstract—An MRI-actuated catheter is a novel robotic catheter system that utilizes the MR scanner for both remote steering and catheter tracking. In order to develop the mathematical model and the planning algorithm of the catheter in parallel to the MR tracking system, an alternative catheter tracking method is needed. This paper presents a catheter tracking algorithm based on the particle filter and the catadioptric camera system. The motion model of the particle filter is based on the quasi-static kinematics of the catheter. The measurement model calculates the weights of the particles according to the normalized cross-correlation of the segmented image from camera and a virtual rendering of the catheter. The efficacy of the tracking algorithm is demonstrates via experimental results.

I. Introduction

The MRI-actuated catheter is a robotic catheter designed to operate while the patient is inside the bore of an MR scanner. Electromagnetic coils attached to the catheter remotely steer the catheter under the magnetic field of the MR scanner when electrical currents are applied to the coils [1]. The MR scanner also provides anatomical images and tracks the catheter during procedures.

In order to validate the model of the catheter and the planning algorithm in parallel to the development of the MR tracking system, an alternative sensing mechanism for obtaining the configurations of the catheter under different actuation currents is needed. A camera is an ideal candidate in this situation because the sensing device has to be placed as far away as possible from the MR scanner for safety reasons. However, the traditional stereo camera system cannot be used here because the distance of the two cameras, and consequently depth perception, is limited by the cylindrical shape of the MR scanner's bore. Fortunately, the problem can be circumvented by replacing the second camera with a mirror placed next to the catheter at 45 degree angle. The mirror provides a side view of the catheter, and effectively serves as a virtual camera. A single camera then records images of the catheter and its reflection in the mirror, which can be used to reconstruct the 3D shape of the catheter. This setup is known in the literature as the catadioptric camera system [2]–[6].

This work was supported in part by the National Science Foundation under grants CISE IIS-1524363, CISE IIS-1563805, ENG IIP-1700839, and National Institutes of Health under grant R01 EB018108.

The authors are with the Department of Electrical Engineering and Computer Science, Case Western Reserve University, Cleveland, OH. They can be reached via email at txg92@case.edu, rcj33@case.edu, and cavusoglu@case.edu, respectively.

This paper presents a catadioptric stereo vision-based tracking algorithm for the MRI-actuated catheter. The algorithm takes the images from the catadioptric camera system as an input, and estimates the configurations of the catheter. The tracking algorithm is an implementation of the particle filter [7], where the quasi-static kinematic model of the catheter [8] serves as the motion model of the particle filter, and the measurement model of the particle filter calculates the weight from the normalized cross-correlations between a segmented catheter image and a virtual rendering of the catheter.

The paper is organized as follows. First, the experimental setup is described in Section II. The tracking algorithm, the motion model, and the measurement model are explained in Section III. Experimental validation of the tracking algorithm is presented in Section IV. Conclusions are given in Section V.

II. EXPERIMENTAL SETUP

The catheter prototype is shown in Fig. 1. The body of the catheter is made of a silicone rubber tube with the outer diameter of 3.2 mm and the length of 104.0 mm (Part number: T2011, QOSINA). The catheter has two actuators, and each actuator has three mutually orthogonal coils. The coils are made of heavy insulated 38-gauge solid core enameled copper wire (Adapt Industries, LLC, Salisbury, MD, USA). Each coil is controlled by one channel on the controller, where Channels 1 and 2 are the side coils of the proximal actuator, Channels 4 and 5 are the side coils of the distal actuator, and Channels 3 and 6 are the axial coils of the proximal and distal actuators, respectively. The rest of the parameters of the catheter prototype are listed in Table I.

The catheter setup is shown in Fig. 2. The catheter is mounted on top of an aquarium that is placed on a foam pad. The mirror is placed on the foam pad next to the catheter at approximately 45 degree angle measured from the side of the aquarium. The calibration pattern in the aquarium and its reflection in the mirror are used to calculate the configuration of the mirror. The black plastic beads hanging from the side of the aquarium and their reflections provide the orientation of the catheter's coordinate system. Nail polish is painted on the catheter as the markers for the tracking algorithm.

Experiments are conducted with the catheter setup placed at the isocenter of a 3 T MR scanner (Skyra, Siemens Medical Solutions, Erlangen, Germany). A 60 fps high definition camera with a resolution of 1080×1920 pixels (Flea3 FL3-U3-32S2C by Point Grey, Richmond, BC, Canada) is used

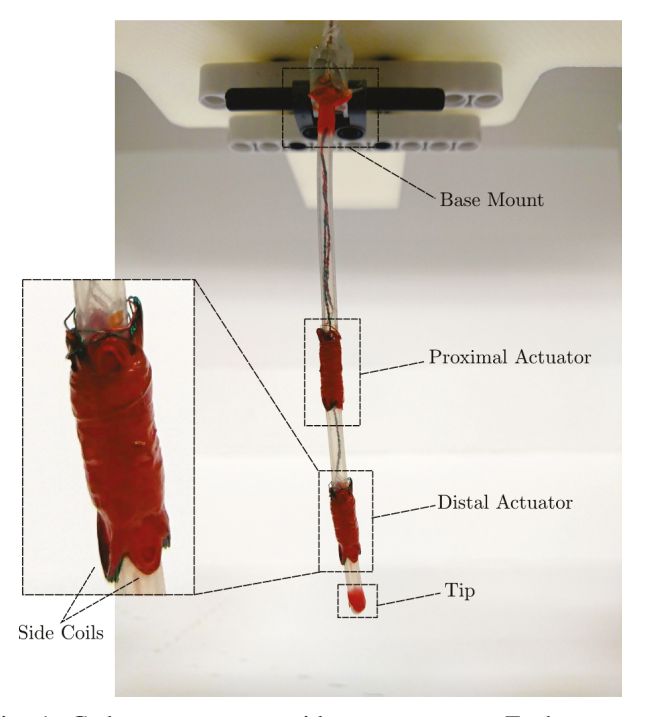


Fig. 1: Catheter prototype with two actuators. Each actuator has an axial and two side coils. The proximal actuator is closer to the base, while the distal actuator is closer to the tip. The catheter is glued to a Lego piece that is attached to the base mount.

TABLE I: Catheter Prototype Parameters

Parameter	Value
Inner diameter (mm)	2.0
Outer diameter (mm)	3.2
Total length (mm)	104.0
Distance of the 1st actuator from the base (mm)	54.0
Distance of the 2nd actuator from the base (mm)	85.2
Winding turns of channel 1	30
Winding turns of channel 2	30
Winding turns of channel 3	100
Winding turns of channel 4	30
Winding turns of channel 5	30
Winding turns of channel 6	100
Surface area of channel 1 (mm ²)	55.0
Surface area of channel 2 (mm ²)	44.2
Surface area of channel 3 (mm ²)	15.6
Surface area of channel 4 (mm ²)	48.0
Surface area of channel 5 (mm ²)	46.2
Surface area of channel 6 (mm ²)	16.0

to capture the images of the catheter during the experiments. For safety reasons, the camera is placed at the far end of the MRI suite, approximately 6 m away from the isocenter of the scanner. Fig. 3 shows the catheter setup and the camera during an experiment. The images from the camera are stored on a laptop connected to the camera via a USB3 cable. Additional information, such as timestamps and actuation indices, are embedded on the top left corner of the image via the GPIO pins.

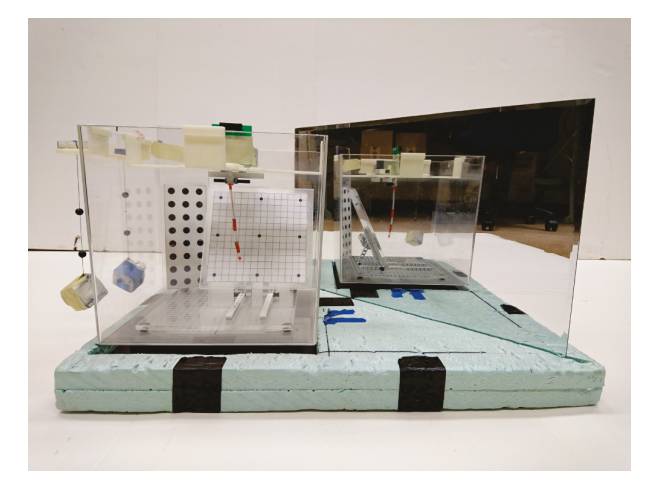


Fig. 2: The experimental setup with the catheter and the mirror mounted on the foam pad. By placing the mirror at an approximately 45 degree angle, the mirror serves and a virtual camera that view the catheter from the side. This setup solves the problem with low depth of field that came with the constraints in the MRI suite. A flat surface mounted is on the bottom of the aquarium tank for surface motion experiments.



Fig. 3: The camera and the catheter setup in the MRI suite. The camera is at the bottom of the image, while the catheter setup is inside the MR scanner's bore. The distance from the camera to the catheter is 6 m.

III. PARTICLE FILTER TRACKING

The particle filter is a nonparametric Bayes filter [7]. Unlike parametric filters, such as the extended Kalman filter or the unscented Kalman filter, the particle filter does not represent the belief using parametric functions. Instead, the particle filter relies on particles, where each particle has a value and a weight, to represent the belief. The value of a particle represents a hypothesis of the state of the system, while the weight indicates how likely that hypothesis is. In the case of catheter tracking, the state of the system is a vector containing the shape parameters of the catheter, denoted by θ .

The pseudo code for the catheter tracking algorithm based

Algorithm 1 Particle update steps in the particle filter

```
1: procedure update_particle(\mathcal{P}_{t-1}, u_t, z_t)
           \mathcal{P}_t = \emptyset
2:
           for all p = (\theta, w) \in \mathcal{P}_{t-1} do
3:
                \theta = \mathtt{motion\_model}(\theta, u_t)
 4:
                 w = \mathtt{measurement\_model}(\theta, z_t)
 5:
           end for
 6:
           for i=1,\cdots,\mathcal{P}_{t-1}.\mathtt{size}() do
 7:
 8:
                p = \mathtt{sample}(\mathcal{P}_{t-1})
 9:
                \mathcal{P}_t.add(p)
           end for
10:
           return \mathcal{P}_t
11:
12: end procedure
```

on the particle filter is shown in Algorithm 1. The algorithm takes as inputs the previous list of particles (denoted by \mathcal{P}_{t-1}), a new actuation (denoted by u_t), and a new measurement (denoted by z_t). The value and the weight of a particle, p, are denoted by θ and w, respectively. There are two main steps in the algorithm, i.e., the prediction and the measurement update steps. In the prediction step, the values of the particles from the previous particle list are updated using the motion model of the system. This happens in Line 4 of the algorithm. In the measurement update step, the weights of the particles are updated using the measurement model of the system. Then a new particle list is created by resampling from the updated particle list, where the chance of a particle being sampled is proportional to the weight of the particle. This happens in Line 5 and Lines 8 to 9, respectively. The remainder of this section explains how prediction and measurement updates are implemented for the catheter tracking algorithm.

A. Motion Model

The motion model describes how the state of the system changes as a function of the previous state and actuation. In this work, the motion model is assumed to be quasi-static, that is the catheter has enough time to reach its equilibrium configuration after each actuation. This is a common assumption for continuum robots in medical applications [9]. A quasi-static configuration of the catheter for a given actuation can be obtained by minimizing the potential energy of the catheter as follows.

$$\min_{\theta} \frac{1}{2} \theta^T K \theta - \sum_{i} m_i g^T p_i(\theta) - \sum_{j} B_j(\theta)^T \mu_j(u_j), \quad (1a)$$

$$s.t. h(\theta) < 0. \tag{1b}$$

The first term in the objective function (1a) is the potential energy due to the internal stiffness of the catheter, where K is the stiffness matrix. The next term is the potential energy due to gravity, where m_i is the mass of the ith rigid body, which can be a link or an actuator, g is the gravity vector, and $p_i(\theta)$ is the center of mass of the i rigid body. The last term is the summation of the potential energy of the magnetic moments from the actuators [10], where $B_i(\theta)$ is the MRI's magnetic

field vector in the jth actuator body frame, μ_j is the magnetic moment of the jth actuator expressed in its body frame, and u_j are the currents sent to the jth actuator.

The inequality constraint (1b) represents the surface the catheter operates on. The constraint is defined such that when the catheter is in contact with the surface, $h(\theta) = 0$, and when the catheter is not in contact, $h(\theta) < 0$. This inequality constraint makes it possible to use the optimization problem (1) to calculate the equilibrium configuration of the catheter both when it is in contact, and when it is free space.

The motion model uses the Jacobian of the implicit function defined by the potential energy minimization problem to calculate a new joint angle vector. Being a linearization, the Jacobian only approximates the minimization problem locally. This locality makes the Jacobian well suited as the motion model of the particle filter, because the unmodeled errors can be included in the particles' values, and the Jacobian will update the values locally. The motion model based on the Jacobian is given by

$$\theta_t = \theta_{t-1} + J_{t-1} (u_t + \rho) + \nu, \tag{2}$$

where $J_{t-1} = \partial \theta_{t-1}/\partial u_{t-1}$ is the Jacobian, ρ is the actuation noise that represents error in actuation model, and ν is the state-space noise that represents other unmodeled errors.

In order to save computational resources, only the Jacobian of the best particle is calculated, and the other particles use the same Jacobian to update its value. The rationale behind this is the fact that good particles most likely have similar values, so their Jacobians will have the same range space. While this may result in errors in the new particle values, remember that noises are added to both actuation and state variables anyway. So, the errors induced by using the same Jacobian can be seen as an additional noise in the motion model.

B. Measurement Model

The measurement model describes the likelihood of a measurement given a state. The measurement for the catheter tracking system is the images from the camera. The measurement model of the catheter tracking system is more complicated when compared to, for example, range-based sensors, because each measurement is a pair of stereo images. Fig. 4 illustrates the processes involved in calculating the weight of a particle from the particle's value and a pair of stereo images. On the image-processing side, a raw image from the camera is first rectified to correct lens distortion. An example of a raw image from the camera is shown in Fig. 5. The distortion coefficients are obtained from the camera calibration images taken at the beginning of the experiment. Then the rectified image is segmented to obtain a gray-scale image, where the parts of the image with the same color as the markers are highlighted. Next, the segmented image is thresholded to obtain the binary image shown in Fig. 6. The binary image will be compared with the images rendered from the values of the particles to obtain the weights for the particles.

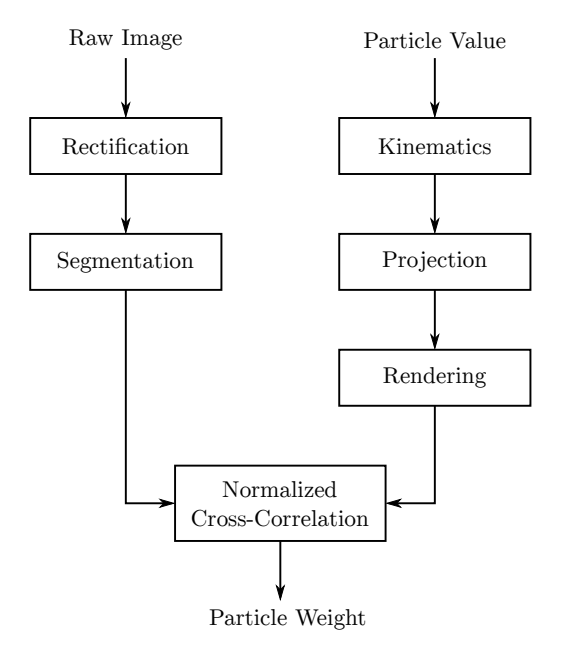


Fig. 4: The image-processing and the rendering procedures involved in calculating the weight of a particle.

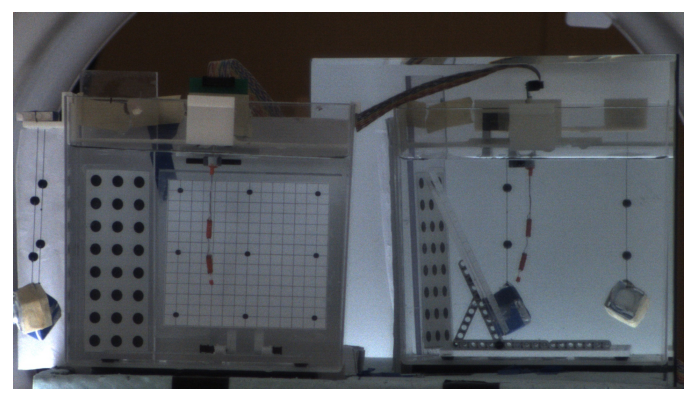


Fig. 5: The raw image obtained from the camera.



Fig. 6: The binary image obtained after the threshold is applied to the segmented image.

The rendering process has the following steps. First the configurations of the markers are calculated from the kinematics of the model, and the particle's value [8]. Next, the configurations of the markers are projected onto the real and mirrored images using the camera projection matrix and the configuration of the mirror. Let points in the real and the mirrored images be denoted by (x_r, y_r) and (x_m, y_m) , respectively. A 3D point in the camera frame, denoted by (X, Y, Z), is projected into points on the real and mirrored images as follows [6], [11],

$$\begin{bmatrix} x_r \\ y_r \end{bmatrix} = \begin{bmatrix} X_r/Z_r \\ Y_r/Z_r \end{bmatrix}, \begin{bmatrix} X_r \\ Y_r \\ Z_r \end{bmatrix} = P \begin{bmatrix} X \\ Y \\ Z \\ 1 \end{bmatrix},$$
 (3a)

$$\begin{bmatrix} x_m \\ y_m \end{bmatrix} = \begin{bmatrix} X_m/Z_m \\ Y_m/Z_m \end{bmatrix}, \begin{bmatrix} X_m \\ Y_m \\ Z_m \end{bmatrix} = PG \begin{bmatrix} X \\ Y \\ Z \\ 1 \end{bmatrix}, \quad (3b)$$

where $P \in \mathbb{R}^{3 \times 4}$ is the camera projection matrix, and $G \in SE(3)$ is the transformation between the real camera to the virtual camera frames. Since it is desirable for the tracking algorithm to be capable of handling occlusions, the links of the model are rendered as well. It is important to render the objects in the correct order to simulate occlusion, because the object that is occluded has to be rendered before the object that is in front. In this work, the process is simplified by assuming that the catheter bends in simple arcs, where the coordinate position of the parts of the catheter along the camera axis changes monotonically. Therefore, the order of rendering can be determined from the direction that the catheter is bending. If the catheter bends away from the camera, the catheter is rendered from the tip to the base. Conversely, if the catheter bends toward the camera, the catheter is rendered from the base to the tip. This order of rendering can be easily generalized if the catheter bends in complex shapes by sorting the parts to be rendered according to their coordinate positions along the camera axis. Finally, Gaussian blur is applied to the rendered image to add measurement uncertainty to the measurement model. Figures 7 shows a rendered image of the catheter.

The similarity between the binary and the rendered images is calculated from their normalized cross-correlation implemented in the matchTemplate function in OpenCV. Let T denote the template, which in this case is the image rendered from the value of a particle, and I denote the binary image. The normalized cross-correlation of the two images, denoted by R, is calculated as follows,

$$R = \frac{\sum_{x,y} (T(x,y) \ I(x,y))}{\left(\sum_{x,y} T(x,y)^2 \ \sum_{x,y} I(x,y)^2\right)^{1/2}},$$
 (4)

where (x, y) is the image coordinates. In order to reduce the computational burden, and more importantly to make the measurement model more selective, the matching score is calculated for the region of interest (ROI) around each marker.

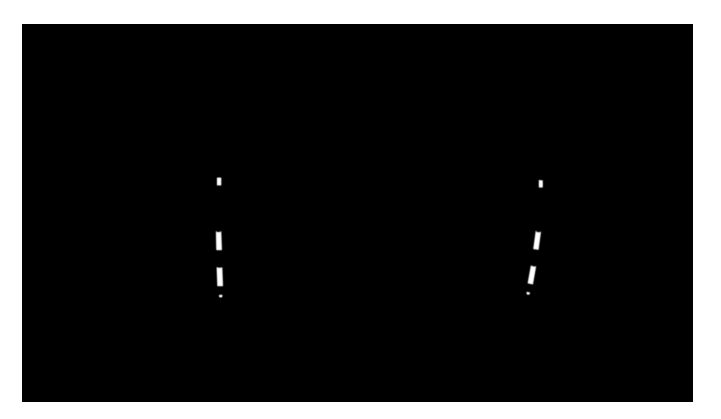


Fig. 7: The rendered image.

The weight of the particle is then defined as the square root of the sum of the matching scores squared. Let R_i denote the normalized cross-correlation between the binary and the rendered images in the ith ROI, then the weight of the particle is calculated as follows,

$$w = \sum_{i} \sqrt{R_i^2}.$$
 (5)

By calculating the matching score of the ROIs instead of the whole image, computational effort is reduced because a much smaller number of pixels have to be processed. The measurement model is also more selective because the baseline similarity from the background the the images is not considered, as a result, the differences between particles are greater.

IV. TRACKING RESULTS

This section presents the experimental results of the tracking algorithm. In the first experiment, the algorithm tracks the catheter when it is at its rest configuration and when it deflects away from the camera. Fig. 8 shows the tracking algorithm locating the catheter when the catheter is at the initial configuration. Fig. 9 shows the catheter being tracked successfully when the catheter deflects away from the camera at approximately 90 degrees, obscuring parts of the catheter's markers. By employing the motion model, the tracking algorithm can track the catheter even when the some of the markers are not clearly visible on one of the images.

In the second experiment, the efficacy of the tracking algorithm is validated by comparing the positions of the catheter's tip from the tracking algorithm with the positions manually obtained from the images. In this experiment, the grid on the surface is replaced with graph paper that serves as an alternative measurement tool for validating the tracking algorithm. The new setup is shown in Fig. 10. This experiment demonstrates the ability of the algorithm in tracking the catheter when the catheter moves on the surface. The catheter first moves toward the surface, then the catheter slides its tip on the surface. The orientation of the surface's coordinate frame with respect to the catheter's coordinate frame written in the axis-angle representation is $[-1.1410, 0, 0]^T$ rad, and

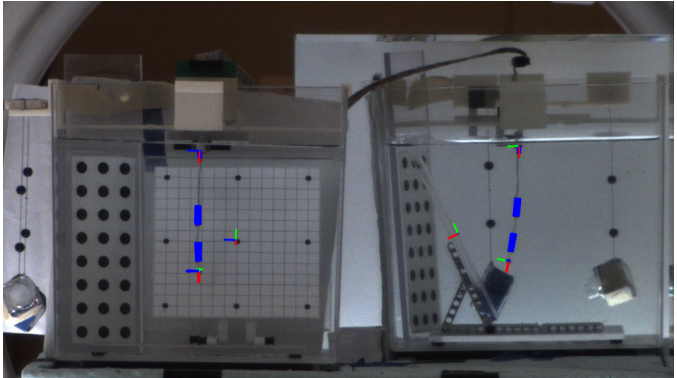


Fig. 8: The catheter being tracked at its initial configuration. The markers are highlighted in blue. The coordinate frames at the catheter's base, the catheter's tip, and the surface origin are rendered with red-green-blue cylinders.

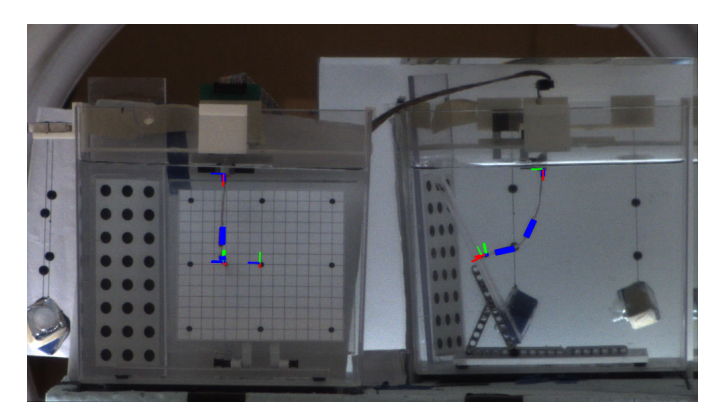


Fig. 9: The catheter being tracked when it bends toward the surface. Note that the tracking algorithm can still track the catheter even when the catheter deflects away from the camera at approximately 90 degrees. The markers are highlighted in blue. The coordinate frames at the catheter's base, the catheter's tip, and the surface origin are rendered with redgreen-blue cylinders.

the position of the surface's origin is $[-5.0, 57.0, 79.5]^T$ mm. ¹ The results from the tracking algorithm and manual tracking are shown in Fig. 11, and the error between the two trajectories is plotted in Fig. 12. Note that the results from the tracking algorithm and manual tracking have similar overall shapes. There seems to be a 2 to 3 mm offset along the surface's *y*-axis between the two trajectories. This could be due to multiple reasons, such as poor lighting causing tip segmentation issue, error in the transformation between the catheter's to the camera's coordinate frame, human error in reading the graph paper, etc. This level of error considered acceptable because it is smaller than the diameter of the catheter, and it is difficult to read graph paper with higher resolution in this lighting condition.

 1 The catheter's coordinate frame is defined at the catheter's base mount with the y-axis and the z-axis aligned with the scanner's magnetic field and gravity, respectively.

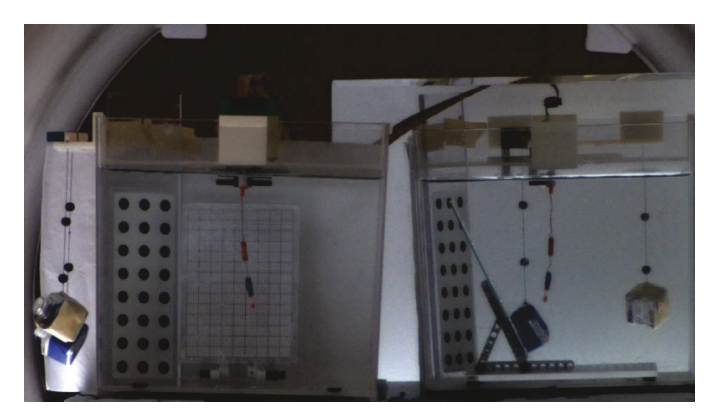


Fig. 10: The catheter setup with the grid on the surface replaced by graph paper. The graph paper serves as an alternative measurement tool for validating the tracking algorithm. The main grid lines in the graph paper are 10 mm apart, and the secondary lines are 2 mm apart.

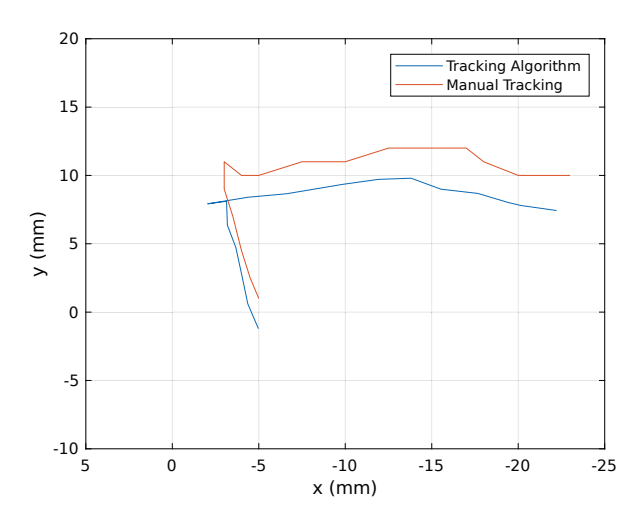


Fig. 11: Tracking result from the tracking algorithm compared with manual tracking result.

V. CONCLUSIONS

This paper presents a catadioptric stereo vision-based tracking algorithm for the MRI-actuated catheter. The tracking algorithm is an implementation of the particle filter, where the motion model is the linearization of the potential energy minimization problem, and the measurement model calculates the weight of a particle from the normalized cross-correlation between an image from the camera and a virtual rendering of the catheter based on the particle's values. The first experimental result shows that the algorithm can track the catheter even when the some markers are not clearly visible on one of the images. The second experiment demonstrates the ability of the algorithm in tracking the catheter performing a surface motion. The presented tracking method is useful in validating the model and planning algorithm of the catheter while the MR tracking system is being developed. The presented tracking method can also be used to validate the MR tracking system.

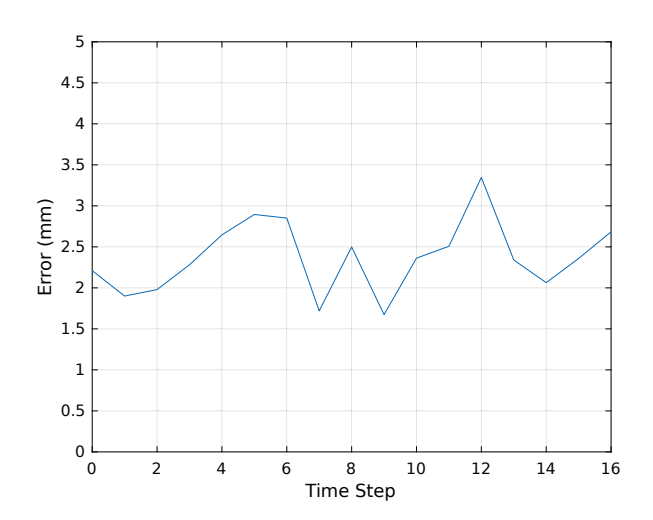


Fig. 12: The error between the results from the tracking algorithm and the manual tracking.

REFERENCES

- N. Gudino, J. A. Heilman, J. J. Derakhshan, J. L. Sunshine, J. L. Duerk, and M. A. Griswold, "Control of intravascular catheters using an array of active steering coils," *Medical Physics*, vol. 38, no. 7, pp. 4215–4224, 2011.
- [2] C. Geyer and K. Daniilidis, "Catadioptric projective geometry," *International Journal of Computer Vision*, vol. 45, no. 3, pp. 223–243, 2001.
- [3] J. Gluckman and S. K. Nayar, "Planar catadioptric stereo: Geometry and calibration," in *IEEE Computer Society Conference on Computer Vision* and Pattern Recognition, vol. 1. IEEE, 1999, pp. 22–28.
- [4] —, "Rectified catadioptric stereo sensors," *IEEE transactions on pattern analysis and machine intelligence*, vol. 24, no. 2, pp. 224–236, 2002
- [5] H.-H. P. Wu, M.-T. Lee, P.-K. Weng, and S.-L. Chen, "Epipolar geometry of catadioptric stereo systems with planar mirrors," *Image and Vision Computing*, vol. 27, no. 8, pp. 1047–1061, 2009.
- [6] R. C. Jackson, T. Liu, and M. C. Çavuşoğlu, "Catadioptric stereo tracking for three dimensional shape measurement of MRI guided catheters," in *IEEE International Conference on Robotics and Automation (ICRA)*, May 2016, pp. 4422–4428.
- [7] S. Thrun, W. Burgard, and D. Fox, Probabilistic Robotics. The MIT Press, Aug 2005.
- [8] T. Greigarn and M. C. Çavuşoğlu, "Experimental Validation of the Pseudo-Rigid-Body Model of the MRI-Actuated Catheter," in *IEEE International Conference on Robotics and Automation (ICRA)*, May 2017, pp. 3600–3605.
- [9] J. Burgner-Kahrs, D. C. Rucker, and H. Choset, "Continuum robots for medical applications: A survey," *IEEE Transactions on Robotics*, vol. 31, no. 6, pp. 1261–1280, 2015.
- [10] D. Dugdale and D. E. Dugdale, Essentials of Electromagnetism. Springer Science & Business Media, 1993.
- [11] R. Hartley and A. Zisserman, Multiple View Geometry in Computer Vision. Cambridge University Press, 2003.